

# On the numerical reliability of nonsmooth autodiff: a MaxPool case study

Ryan Boustany\*

January 8, 2024

## Abstract

This paper considers the reliability of automatic differentiation (AD) for neural networks involving the nonsmooth MaxPool operation. We investigate the behavior of AD across different precision levels (16, 32, 64 bits) and convolutional architectures (LeNet, VGG, and ResNet) on various datasets (MNIST, CIFAR10, SVHN, and ImageNet). Although AD can be incorrect, recent research has shown that it coincides with the derivative almost everywhere, even in the presence of nonsmooth operations (such as MaxPool and ReLU). On the other hand, in practice, AD operates with floating-point numbers (not real numbers), and there is, therefore, a need to explore subsets on which AD can be *numerically* incorrect. These subsets include a bifurcation zone (where AD is incorrect over reals) and a compensation zone (where AD is incorrect over floating-point numbers but correct over reals). Using SGD for the training process, we study the impact of different choices of the nonsmooth Jacobian for the MaxPool function on the precision of 16 and 32 bits. These findings suggest that nonsmooth MaxPool Jacobians with lower norms help maintain stable and efficient test accuracy, whereas those with higher norms can result in instability and decreased performance. We also observe that the influence of MaxPool’s nonsmooth Jacobians on learning can be reduced by using batch normalization, Adam-like optimizers, or increasing the precision level.

## 1 Introduction

Nonsmooth neural networks are trained using optimization algorithms [10, 14] based on backpropagation and automatic differentiation (AD) [45, 43, 3]. AD is a crucial tool in contemporary learning architectures as it allows for fast differentiation [5, 21]. It is implemented in popular machine learning libraries such as TensorFlow [1], PyTorch [41], and Jax [11]. Although the validity domain of AD is theoretically limited to smooth functions [21], it is commonly used for nonsmooth functions [4, 5, 7]. The behavior of nonsmooth AD has been investigated in previous studies [21, 20, 22, 2, 31, 18, 19, 8, 5].

**MaxPool: a nonsmooth operation** Introduced by Yamaguchi et al. [47], MaxPool is a common operation in convolutional neural networks (CNN), which are a type of network often used for image classification [47, 35, 33, 34, 48]. MaxPool reduces the spatial dimensions of a feature map by selecting the maximum value within specific patches. MaxPool can produce nonsmoothness when it is applied to uniform pixel values. MaxPool frequently selects arbitrary maximum values among identical pixels at image edges (refer to Appendix A.2 for an illustration). Different choices of MaxPool’s nonsmooth Jacobians have a variational sense. In this paper, the term *MaxPool-derived program* refers to a specific choice of a MaxPool nonsmooth Jacobian.

**Various types of nonsmooth AD errors:** We carry out a small experiment using PyTorch [41] to investigate the behavior of the nonsmooth max function, defined as  $\max: x \mapsto \max_{1 \leq i \leq 4} x_i \in \mathbb{R}$ . We implement two max function programs with different derivative implementations:  $\max_1$  and  $\max_2$

---

\*Toulouse School of Economics, University of Toulouse Capitole, Thales LAS France. Toulouse, France.

(see Appendix A.1 for more details). We define program zero as  $\text{zero}: t \mapsto \max_1(t \times x) - \max_2(t \times x)$ , where  $\text{zero}'$  is its associated AD output. As mathematical functions, both  $\max_1$  and  $\max_2$  output the same value, while zero always outputs 0. However, when using AD and floating-point numbers, we observe an unexpected behavior:  $\text{zero}'(t) \neq 0$  for some  $t \in \mathbb{R}$ . In Table 1, we present an analysis

$t$					$\text{zero}'(t)$						
					$-10^{-3}$	$-10^{-2}$	$-10^{-1}$	0	$10^1$	$10^2$	$10^3$
$x =$	1.0	2.0	3.0	4.0	0.0	0.0	0.0	-1.5	0.0	0.0	0.0
$x =$	1.4	1.4	1.4	1.4	$10^{-7}$	$10^{-7}$	$10^{-7}$	$10^{-7}$	$10^{-7}$	$10^{-7}$	$10^{-7}$

Table 1: Overview of numerical AD errors for the zero program with 32 bits precision.

of AD errors for the zero program, highlighting the impact of using AD with floating-point numbers. The first row shows a significant error for  $x = [1.0 \ 2.0 \ 3.0 \ 4.0]$ , where  $\text{zero}'(0) = -1.5$ , but the true derivative is for  $t \neq 0$ . In the second row, with  $x = [1.4 \ 1.4 \ 1.4 \ 1.4]$ , a configuration of equal numbers often encountered in practice (for image classification tasks, refer to Appendix A.2). In this setting, formal computations over real numbers give  $\text{zero}'(t) = 0$  for every  $t \in \mathbb{R}$ . Yet, with floating-point arithmetic, we observe AD variations of low magnitude. Indeed, for all  $t$  considered in Table 1, we have  $\text{zero}'(t) = 5.96 \times 10^{-8}$  (rounded to  $10^{-7}$  in Table 1), which is close to the machine precision with 32 bits precision. This phenomenon occurs due to arithmetic limits. In general,  $t$  represents a neural network parameter, and  $x$  is an input image with a specific pixel area with identical values (e.g., MNIST dataset- refer to Appendix A.2). Note that these phenomena observed in Table 1 are not caused by the nonsmooth multivariate nature of the max function and can also be replicated using only the nonsmooth univariate ReLU operation. Refer to Appendix A.3 for more details.

**Reals vs floating-point numbers:** Over reals, AD outputs derivatives for nondifferentiable functions, except for a Lebesgue measure-zero subset of inputs [8, 9]. On the other hand, as reported in Table 1, floating-point arithmetic can thicken subsets where AD is incorrect [4]. In Section 3, we try to identify numerically two network parameter subsets where AD is incorrect: the *bifurcation zone* with considerable amplitude variations of AD and the *compensation zone* with minor amplitude variations near machine precision, which is due to rounding schemes used for inexact arithmetics over the reals (e.g., non-associativity). From our experiments, in a 64-bit network featuring MaxPool, the compensation zone occupies the entire parameter space. At 32 bits, both compensation and bifurcation zones share the parameter space. In a 16-bit setting, the bifurcation zone appears to occupy the entire parameter space.

**Implications for learning dynamics:** In Section 4, we investigate the impact of different nonsmooth MaxPool Jacobians on learning. At 32-bit precision, various nonsmooth Jacobians yield similar test accuracy. However, high-norm Jacobians lead to lower accuracy due to unstable training or gradient issues. Training in 16-bit precision, active topic research [46, 28, 13, 23], shows greater sensitivity to nonsmooth MaxPool Jacobians used. The sensitivity to this effect depends highly on the problem, particularly the network structure, the dataset, and the precision level. We also observe that both batch normalization [29] and the Adam optimizer [32] mitigate this effect. All experiments were done using PyTorch [41], and our code is publicly available: <https://github.com/ryanboustany/MaxPool-numerical>.

**Related works and contributions:** Recent works show that for a broad class of programs using nonsmooth functions, AD is incorrect at most on a Lebesgue measure-zero subset of the input domain of a program [8, 38]. These prior works consider AD over real numbers. Yet, in practice, inputs to a program are always machine-representable numbers, such as floating-point numbers. Recently, Lee et al. [37] studied the correctness of AD when the parameter space of a neural network consists uniquely of machine-representable numbers and for a particular class of neural networks, which

does not generalize neural networks featuring MaxPool operation. Numerical experiments in [4] investigate the effect of  $\text{ReLU}'(0)$  choice on AD and neural network training output. They empirically studied *the bifurcation zone* for ReLU neural networks: the set of the network parameters on which the output of AD is incorrect. However, they do not consider the case where AD is incorrect over floating-point numbers but correct over real numbers (e.g., last line in Table 1). Thus, our paper introduces *the compensation zone* where AD is incorrect over floating-point numbers but correct over reals. We investigate the numerical reliability of AD for MaxPool-based neural networks across different precision levels (16, 32, and 64 bits). We also show that the numerical observation of the compensation zone varies with the structure of the neural network and is independent of whether nonsmooth functions used are univariate or multivariate. Finally, we conduct an empirical study to investigate the impact of nonsmooth MaxPool Jacobians on the stability and performance of training.

**Organization of the paper:** In section 2, we discuss the elements of nonsmooth backpropagation, and define the subsets of network parameters - bifurcation, compensation, and regular zone. We also introduce nonsmooth MaxPool Jacobians and their theoretical implications for backpropagation, based on [8, 9]. In Section 3, we describe the numerical bifurcation and compensation zone, and the factors that influence their importance. This will be done using convolutional neural networks on the MNIST-CIFAR10 datasets. In Section 4, we present detailed experiments on neural network training. Additionally, you can find further findings in Appendix C.

## 2 Nonsmooth AD in neural networks with MaxPool

### 2.1 Preliminaries and notations

For supervised training in neural networks, we have a training set  $(x_i, y_i)_{i=1}^N$ , where  $x_i$  is an input and  $y_i$  is its corresponding label. We use a neural network function  $f$  to produce predictions  $\hat{y}_i = f(x_i, \theta)$ , where  $\theta$  are the network’s parameters. A loss function  $\ell$  measures the discrepancy between predicted and true labels. To improve the predictions, the goal is to minimize an empirical loss function  $L$  over the training set such as:

$$\min_{\theta \in \mathbb{R}^p} L(\theta) := \frac{1}{N} \sum_{i=1}^N \ell(\hat{y}_i, y_i). \quad (1)$$

For all  $i \in \{1, \dots, N\}$  and  $\theta \in \mathbb{R}^p$ , Equation (1) can be expressed with  $\ell(\hat{y}_i, y_i) = l_i(\theta)$ , where  $l_i : \mathbb{R}^p \rightarrow \mathbb{R}$  represents a composition of  $M$  elementary functions as follows:

$$l_i(\theta) = g_{i,M} \circ g_{i,M-1} \circ \dots \circ g_{i,1}(\theta). \quad (2)$$

Equation (2) encompass common neural architectures representation including feed-forward [42], convolutional [36], and recurrent networks [26]. Throughout the paper, we consider elementary functions that are locally Lipschitz semialgebraic (or definable), which are ubiquitous in nonsmooth neural networks (see [8, 9]). Note that the functions  $g_{i,j}$  encompass operations like linear transformations, ReLU function, MaxPool, convolutions with filters, or softmax for multi-class classification.

### 2.2 Nonsmooth AD framework

Training nonsmooth neural networks [8, 7, 5, 6, 15] is challenging due to the need to compute subgradients from Equation (1). Major machine learning tools such as TensorFlow [1], PyTorch [41], and Jax [11] address this issue using automatic differentiation, referred to here as backprop [43, 3]. They apply differential calculus to nonsmooth items, often replacing derivatives with *Clarke Jacobians* [12]. Given a locally Lipschitz continuous function  $F : \mathbb{R}^p \rightarrow \mathbb{R}^q$ , the *Clarke Jacobian* of  $F$  is defined as:

$$\text{Jac}^c F(x) = \text{conv} \left\{ \lim_{k \rightarrow +\infty} \text{Jac} F(x_k) : x_k \in \text{diff}_F, x_k \xrightarrow{k \rightarrow +\infty} x \right\} \quad (3)$$

where  $\text{diff}_F$  represents the full measure set where  $F$  is differentiable and  $\text{Jac } F$  is the standard Jacobian of  $F$ . A selection  $v$  in  $\text{Jac}^c F$  is a function  $v: \mathbb{R}^p \rightarrow \mathbb{R}^{p \times q}$  such that, for all  $x \in \mathbb{R}^p$ ,  $v(x) \in \text{Jac}^c F(x)$ . If  $F$  is  $C^1$ , the only possible selection is  $v = \text{Jac } F$ .

**Definition 1 (Calculus model, programs and nonsmooth AD)** Let  $l$  be a composition function evaluated at  $\theta \in \mathbb{R}^p$ , as specified in Equation (2). A sequence of sub-programs can characterize a program  $P$  that implements  $l$ :

- Elementary programs:  $\{g_j\}_{j=1}^M$  such that  $l(\theta) = g_M \circ g_{M-1} \circ \dots \circ g_1(\theta)$ .
- Derived programs:  $\{v_j\}_{j=1}^M$  where each  $v_j(w) \in \text{Jac}^c g_j(w)$  at point  $w = g_{j-1} \circ \dots \circ g_1(\theta)$ .

Then, the backprop algorithm automates applying differential calculus rules as follows:

$$\text{backprop}[P](\theta) = v_M(g_{M-1} \circ \dots \circ g_1(\theta)) \cdot v_{M-1}(g_{M-2} \circ \dots \circ g_1(\theta)) \cdot \dots \cdot v_1(\theta). \quad (4)$$

In practice, AD libraries [1, 41, 11] implement dictionaries (see for e.g. [5]) containing conjointly elementary programs and derived programs which efficiently computes the quantities defined in Equation (4).

**Remark 1** As seen in Section 1 with the zero program, various programs can implement a unique composition function  $l$ . Each elementary program  $g_j$  in the composition (see Definition 1) can be associated with different derived programs  $v_j$ . Specifically, for any  $j = 1, \dots, M$  and  $w = g_{j-1} \circ \dots \circ g_1(\theta)$ , all selections  $v_j(w)$  from the Clarke Jacobian of  $g_j(w)$  can be used.

**Example 1** The Clarke subdifferential of  $\text{ReLU}(t) = \max(0, t)$  at  $t$  is 0 for  $t < 0$ , 1 for  $t > 0$ , and the interval  $[0, 1]$  for  $t = 0$ . All derived program that implements  $\text{ReLU}'(0) = s$  with  $s \in [0, 1]$  can be used for backprop and have a variational bear.

**Definition 2 (Backprop set)** Let  $l$  denote a composition function evaluated at  $\theta \in \mathbb{R}^p$ , as specified in Equation (2). We define  $J(\theta)$  as the function that encompasses the set of all possible backprop outputs through all programs implementing  $l(\theta)$  as in Definition 1:

$$J(\theta) = \{\text{backprop}[P](\theta) : P \text{ is a program implementing } l(\theta)\}. \quad (5)$$

**Remark 2** For a composition function  $l$  composed by  $C^1$  elementary programs  $\{g_j\}_{j=1}^M$ ,  $J(\theta)$  is a singleton for all  $\theta \in \mathbb{R}^p$ . For locally Lipschitz semialgebraic (or definable) elementary programs  $\{g_j\}_{j=1}^M$ : Equation (4) is always an element within the backprop set.

**Remark 3** The chain rule, essential for AD, often fails with Clarke subgradients. Hence, the backprop set might differ from the Clarke subdifferential [12]. For example, the Clarke subdifferential of  $2\text{ReLU}(x) - \frac{1}{3}\text{ReLU}(-x)$  at  $x = 0$  is  $[\frac{1}{3}, 2]$ , whereas backprop outputs 0 (with  $\text{ReLU}'(0) = 0$ ).

### 2.3 Network parameters subsets

Recently, Bertoin et al. [4] conducted a numerical analysis of the bifurcation zone for ReLU networks. This zone represents the set of network parameters where the output of AD using  $\text{ReLU}'(0) = 0$  differs from that using  $\text{ReLU}'(0) = 1$ . However, the authors [4] did not include an examination of the subset of network parameters where the backprop set is theoretically a singleton, and AD produces incorrect results due to floating-point arithmetic (as shown in Table 1). To address the issue of incorrect AD, we introduce the concept of a compensation zone for more accurate analysis.

**Definition 3 (Compensation, bifurcation and regular zones)** For each  $i = 1, \dots, N$ , let  $l_i$  denote a composition function evaluated at  $\theta \in \mathbb{R}^p$  and  $J_i(\theta)$  denote the backprop set associated as detailed in Definition 2. We define the following network parameters subsets of  $\mathbb{R}^p$ :

$$\Theta_R = \{\theta \in \mathbb{R}^p : \forall i, j \in \{1, \dots, N\} \times \{1, \dots, M\}, \text{Jac}^c g_{i,j}(w) \text{ is a singleton}\}, \quad (6)$$

$$\Theta_C = \{\theta \in \mathbb{R}^p \setminus \Theta_R : \forall i \in \{1, \dots, N\}, J_i(\theta) \text{ is a singleton}\}, \quad (7)$$

$$\Theta_B = \{\theta \in \mathbb{R}^p \setminus \Theta_R : \exists i \in \{1, \dots, N\} \text{ such that } J_i(\theta) \text{ is not a singleton}\}. \quad (8)$$

where  $w = g_{i,j-1} \circ \dots \circ g_{i,1}(\theta)$ ,  $\Theta_R$  is the regular zone,  $\Theta_C$  the compensation zone and  $\Theta_B$  the bifurcation zone.

The mathematical tools of Proposition 1 are conservative fields developed in [8]. This proposition implies that theoretically (assuming exact arithmetic over the reals), the backprop set is almost everywhere a singleton. The proof is given in Appendix B.

**Proposition 1** Let  $\Theta_R$ ,  $\Theta_B$ , and  $\Theta_C$  be subsets in  $\mathbb{R}^p$  as in Definition 3. Then, we have

- $\Theta_R$ ,  $\Theta_B$ , and  $\Theta_C$  form a partition of  $\mathbb{R}^p$ .
- $\Theta_B$  is a Lebesgue null measure set.

**Remark 4 (Backprop returns a gradient a.e.)** Let  $\theta \in \mathbb{R}^p$  and  $P$  be a program implementing a composition function  $l(\theta)$  as in Definition 1. Then  $\text{backprop}[P](\theta) = \nabla l(\theta)$  almost everywhere.

## 2.4 MaxPool-derived programs

**Definition 4 (Clarke Jacobian of matrix's maximum function)** Let  $X$  be a  $m \times n$  real matrix and  $F_s$  be a function such that  $F_s(X) = \max_{1 \leq i \leq m, 1 \leq j \leq n} X_{ij} \in \mathbb{R}$ , where  $s := m \times n$  denotes the size of  $X$ . The Clarke Jacobian of  $F_s$  at the point  $X$  is:

$$\text{Jac}^c F_s(X) = \text{conv} \left( \bigcup_{(i,j) \in A(X)} E_{ij} \right), \quad (9)$$

where  $A(X) := \{(i,j) \in \{1, \dots, m\} \times \{1, \dots, n\} : F_s(X) = X_{ij}\}$  is the active set and  $E_{ij}$  is an  $m \times n$  matrix with all entries equal to 0 except for the  $(i,j)$ -th entry which is 1.

**Definition 5 (MaxPool operation)** Let  $X \in \mathbb{R}^{p \times q}$  be a real matrix, and  $s := m \times n$  be the size of a pooling window such that  $p \geq m$  and  $q \geq n$ . For each  $i \in \{0, \dots, \lfloor \frac{p}{m} \rfloor - 1\}$  and  $j \in \{0, \dots, \lfloor \frac{q}{n} \rfloor - 1\}$ , we define a submatrix  $X_{i,j}$  of  $X$ , of size  $m \times n$  as follows:

$$X_{i,j} := \{X_{kl} : m \times i \leq k < m \times (i+1), n \times j \leq l < n \times (j+1)\}, \quad (10)$$

where  $k$  and  $l$  are the indices of the entries in  $X$ , in the lexicographic order. The MaxPool operation output a matrix  $Y \in \mathbb{R}^{\lfloor \frac{p}{m} \rfloor \times \lfloor \frac{q}{n} \rfloor}$  where  $Y_{ij} = F_s(X_{i,j})$  for all  $i \in \{0, \dots, \lfloor \frac{p}{m} \rfloor - 1\}$  and  $j \in \{0, \dots, \lfloor \frac{q}{n} \rfloor - 1\}$ . Finally, the MaxPool Clarke Jacobian at point  $X$ , denoted as  $\text{Jac}^c \text{MaxPool}(X)$ , can be obtained by replacing each submatrix  $X_{i,j}$  in  $X$  with  $\text{Jac}^c F_s(X_{i,j})$ .

**Definition 6 (MaxPool-derived programs)** Let  $X_{i,j} \in \mathbb{R}^{m \times n}$  be a submatrix of  $X$  as defined in Definition 5. We define different MaxPool-derived programs, which are selections of the Clarke Jacobian of the matrix's maximum function (see Definition 4 and Section 2.2).

- **Native:** This program selects only the first indice  $(i_1, j_1)$  (in the lexicographic order) from the active set  $A(X_{i,j})$  in Definition 4 and output  $E_{i_1 j_1}$ . Autograd libraries like PyTorch [41] and TensorFlow [1] use this implementation.
- **Minimal:** This program selects all indices in the active set  $A(X_{i,j})$  and returns the following element within Equation (9):

$$\frac{1}{|A(X_{i,j})|} \sum_{(k,l) \in A(X_{i,j})} E_{kl},$$

where  $|A(X_{i,j})|$  denotes the cardinality of  $A(X_{i,j})$ . We called it "minimal" as it yields the smallest norm element within Equation (9).

- **Hybrid:** This program combines native and minimal, defined by parameter  $\beta > 0$ , and is expressed as follows:

$$(1 - \beta) \times E_{i_1 j_1} + \beta \times \left( \frac{1}{|A(X_{i,j})|} \sum_{(k,l) \in A(X_{i,j})} E_{kl} \right),$$

where  $(i_1, j_1)$  is the first indices (in the lexicographic order) in  $A(X_{i,j})$ .

**Remark 5** The hybrid MaxPool-derived program implements a selection of the MaxPool Clarke Jacobian for all  $\beta \in [0, 1]$  and a selection of a conservative Jacobian (refer to [8]) for other  $\beta$  values.

### 3 Numerical AD with MaxPool-derived programs

In this section, we numerically investigate network parameter subsets from Definition 3 over several floating-point precision in the context of neural networks involving nonsmooth MaxPool operation. Note that the numerical bifurcation zone defined in [4] does not hold for our analysis with MaxPool-derived programs. Indeed, as seen in Table 1, we also have to consider minor amplitude AD errors where AD is incorrect over floating-point numbers but correct over real numbers. Thus, we analyze the numerical bifurcation and compensation zone through numerical proposals. In the following, we use notation from Section 2.1 and 2.2.

#### 3.1 A numerical criteria for the bifurcation and compensation zone

**Definition 7 (Backprop variation)** Let  $(B_q)_{q \in \mathbb{N}}$  denote a sequence of mini-batches, each with a size  $|B_q| \subset \{1, \dots, N\}$ , for all  $q$ . Let  $P = \{P_i\}_{i=1}^N$  and  $Q = \{Q_i\}_{i=1}^N$  be two programs implementing a neural network using different derived programs (e.g., native vs. minimal). More precisely, for each  $i = 1, \dots, N$ ,  $P_i$  and  $Q_i$  implement a composition function  $l_i$  as in Definition 1. We define the backprop variation between  $P$  and  $Q$  for  $M$  experiments with random parameters  $\{\theta_m\}_{m=1}^M$  as:

$$D_{m,q}(P, Q) = \left\| \text{backprop} \left[ \sum_{i \in B_q} P_i(\theta_m) \right] - \text{backprop} \left[ \sum_{i \in B_q} Q_i(\theta_m) \right] \right\|_1. \quad (11)$$

Recently, Bertoin et al. [4] investigated a numerical bifurcation zone  $S_{01}$  in the context of ReLU-derived programs. For each  $i = 1, \dots, N$ , let  $R_i^0$  (under  $\text{ReLU}'(0) = 0$ ) and  $R_i^1$  (under  $\text{ReLU}'(0) = 1$ ) be two programs implementing a composition function  $l_i$  as in Definition 1.

$$S_{01} = \{ \theta \in \mathbb{R}^P : \exists i \in \{1, \dots, N\}, \text{backprop}[R_i^0](\theta) \neq \text{backprop}[R_i^1](\theta) \}. \quad (12)$$

This numerical bifurcation zone  $S_{01}$  does not extend to our case of MaxPool-derived programs, as we also consider AD errors from the numerical compensation zone.

**A 32 bits MNIST experiment:** To convey this fact, we carried out a small experiment in PyTorch [41]. Let  $P$  and  $Q$  be two programs implementing a LeNet-5 network on the MNIST dataset with native and minimal MaxPool-derived programs, respectively. For a sanity check, let  $\tilde{P}$  be a copy of  $P$ . We compute the backprop variation (see Definition 7) between  $P$  and  $\tilde{P}$  and between  $P$  and  $Q$ . We control all sources of divergence in our implementation using deterministic computation. Results are reported in Figure 1 and the experiment was run on a CPU under 32 bits precision. First, we observe no backprop variation between  $P$  and  $\tilde{P}$ , which shows that we have controlled all possible sources of divergence. Second, while no backprop variation between  $P$  and  $Q$  is expected (Proposition 1), we observe that  $D_{m,q}(P, Q) > 0$  for all  $m, q$ . More precisely, we observe two types of backprop variation. The first one has small variations that oscillate between  $10^{-7}$  and  $10^{-8}$ , roughly the value of machine precision in 32 bits and accounting for 98.78% of network parameters. These

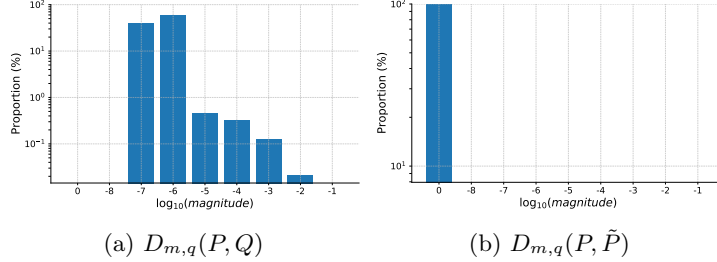


Figure 1: Histogram of backprop variation  $D_{m,q}$  between  $P$ , and  $\tilde{P}$  and between  $P$  and  $Q$  for a LeNet-5 network on MNIST (128 mini-batch size) under 32 bits precision. We run  $M = 1000$  experiments.

variations seem to reflect the numerical compensation zone, where non-associative floating-point arithmetic and cumulative rounding errors impact backprop. The second one with large variations up to  $10^{-3}$ , representing 1.22% of network parameters. These variations likely correspond to the numerical bifurcation zone. Our experiment produced different results than those in [4]. The authors found either significant backprop divergences leading to bifurcation or no variation.

**An heuristic for the numerical bifurcation zone:** As seen in Figure 1, we observe numerically two types of backprop variation, one potentially from the numerical bifurcation zone similar to what has been discussed in [4], and the other attributable to floating-point arithmetic and numerical errors (compensation errors). To investigate two numerical phenomena, we need to compare the observed variations in magnitudes of backprop (shown in Figure 1) with known variations. These known variations arise from two sources. The first source is due to nondeterministic GPU calculations, which are explained in more detail in Appendix A.6.1. The second source is due to backprop variations related to ReLU-derived programs, as reported in 16 and 32-bit floating-point in [4]. This method proposes a numerical bifurcation zone without assuming the existence of separate numerical bifurcation and compensation zones. Let  $\omega$  represent floating-point precision and  $f$  denote a neural network such as LeNet-5, VGG, or ResNet.

**A threshold with non-deterministic GPU calculations:** We establish a threshold  $\tau_{f,\omega}^1$  that quantifies the highest backprop variation resulting from the non-deterministic GPU calculations (see Appendix A.6.1):

$$\tau_{f,\omega}^1 = \max_{1 \leq m \leq M, 1 \leq q} D_{m,q}(P, \tilde{P}) \tag{13}$$

where  $P$  and  $\tilde{P}$  implement the same neural network  $f$  under the same MaxPool-derived program (e.g., native or minimal). Refer to Figure 2 for an illustration. We observe no backprop variation with  $\omega = 16$ , as PyTorch can turn off some nondeterministic GPU operations (e.g., convolution operations).

**A threshold with ReLU-derived programs:** Let  $R^0$  (under  $\text{ReLU}'(0) = 0$ ) and  $R^1$  (under  $\text{ReLU}'(0) = 1$ ) be two programs implementing a neural network  $f$  as in Definition 1. We define a threshold  $\tau_{f,\omega}^2$  based on backprop variation such as:

$$\tau_{f,\omega}^2 = \min_{1 \leq m \leq M, 1 \leq q} \{D_{m,q}(R^0, R^1) : D_{m,q}(R^0, R^1) > 0\}, \tag{14}$$

See Figure 3 for an illustration. In this experiment, we enforce deterministic operations on the GPU. In Figure 3, we observe two types of backprop variations: high divergence amplitude or no variation; the divergences are the same magnitude as the more significant variations observed in Figure 1. These could potentially delineate a numerical bifurcation zone. On the other hand, the variations seen in Figure 2, which correspond to nondeterministic GPU calculations, match the more minor variations

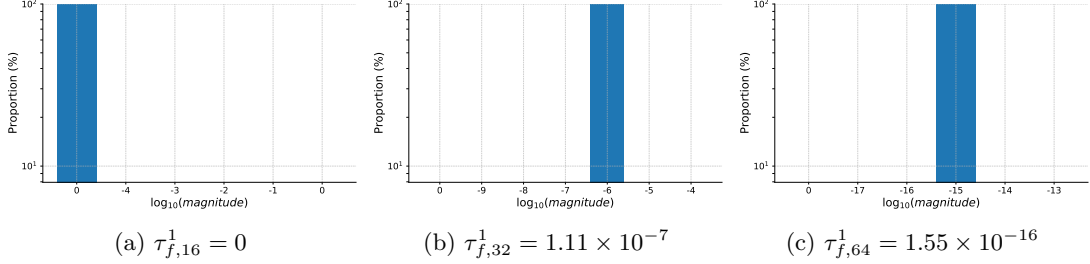


Figure 2: Histogram of backprop variation under nondeterministic GPU operations, where  $f$  is a LeNet-5 network on MNIST with batch size 128 for  $K = 1000$  experiments.

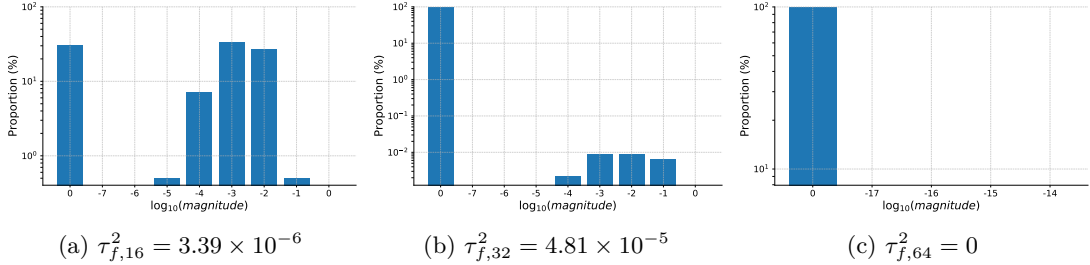


Figure 3: Histogram of backprop variation with ReLU-derived programs, where  $f$  is a LeNet-5 network on MNIST with batch size 128,  $K = 1000$  experiments.

near machine precision in Figure 1. Using these hypotheses, we propose a numerical bifurcation zone; different thresholds are used for different precisions due to hardware constraints.

**Criteria 1 (Numerical bifurcation zone)** For a neural network  $f$  and a floating-point precision  $\omega$ , let  $\tau_{f,\omega}$  be a fixed threshold (for e.g.  $\tau_{f,\omega}^1, \tau_{f,\omega}^2$ ). The numerical bifurcation zone can be formulated as:

$$S(\tau_{f,\omega}) = \{\theta \in \mathbb{R}^P : \exists i \in \{1, \dots, N\}, \|\text{backprop}[P_i](\theta) - \text{backprop}[Q_i](\theta)\|_1 > \tau_{f,\omega}\} \subset \Theta_B. \quad (15)$$

where for all  $i \in \{1, \dots, N\}$ ,  $P_i$  and  $Q_i$  are two programs implementing a composition function  $l_i$  (associated to a neural network  $f$ ) using minimal and native MaxPool-derived programs, respectively.

Table 4 in Appendix A.6 summarizes different threshold values for various networks across datasets using 16-bit, 32-bit, and 64-bit floating-point precisions. Note that these thresholds serve as numerical heuristics and depend highly on factors such as network parameters initialization, dataset, and neural network architectures.

**Compensation zone and network structure:** The neural network structure determines the compensation zone’s existence and is not dependent on whether the elementary programs in Definition 1 are univariate or multivariate. For instance, ReLU-derived programs can also produce the same compensation errors as demonstrated in Table 1 (refer to Appendix A.3). Convolutional neural networks such as VGG or ResNet can be implemented with ReLU activation function replacing the MaxPool program. It can be done by using the equation  $2 \max(x, y) = (x + y) + (\text{ReLU}(x) - \text{ReLU}(-y)) + (\text{ReLU}(y) - \text{ReLU}(-x))$ . When this is done, the bifurcation zone described in [4] with MaxPool implemented by ReLU-derived programs no longer applies. On the other hand, replacing MaxPool with a NormPool, a nonsmooth multivariate operation that implements the Euclidean norm instead of the maximum, does not yield compensation errors. We verify this empirically through similar experiments as in Figure 1. More details are available in the Appendix A.4.

### 3.2 Volume of the numerical bifurcation zone

We estimated the volume of the numerical bifurcation zone with Monte Carlo sampling across various networks and conditions to Criteria 1. Refer to Appendix A.6.3 for more details. In these experiments, we use the thresholds  $\tau_{f,16}^2$ ,  $\tau_{f,32}^1$  and  $\tau_{f,64}^1$  for all neural network  $f$ , as defined in Equation (13) and (14).

**Experimental setup:** We generate a set of network parameters  $\{\theta_m\}_{m=1}^M$  randomly using Kaiming-Uniform initialization [24]. Here,  $M = 1000$ . Then, we iterate over the entire CIFAR10 dataset to estimate the proportion of  $\theta_m$  in the numerical bifurcation zone  $S$  defined in Criteria 1 (as shown in Equation (18)) and the proportion of impacted mini-batches (as shown in Equation (19)).

**Impact of floating-point precision:** Using a VGG11 network on CIFAR10 dataset, we evaluate the volume of  $S$  (Equation (18)) for different floating-point precision. Table 2 shows that with 16-bit and 32-bit precision, all sampled network parameters are in  $S$ , while none are in  $S$  with 64-bit precision. The affected mini-batches have a 46% impact at 32 bits and 100% at 16 bits. These results show that floating-point precisions influence the effects of MaxPool-derived programs during backprop.

Floating-point precision	16 bits	32 bits	64 bits
Proportion of $\{\theta_m\}_{m=1}^M$ in $S$	100%	100%	0%
Proportion of impacted mini-batches	100%	46.67%	0%

Table 2: Impact of  $S$  according to floating-point precision using a VGG11, on CIFAR10 dataset and  $M = 1000$  experiments. The first line represents network parameters  $\theta_m$  in  $S$ , while the second measured the proportion of affected mini-batches falling in  $S$ .

**Impact of mini-batch size:** We estimate the impact of the mini-batch size by computing the proportion of affected mini-batches in  $S$ , using the VGG11 network on the CIFAR10 dataset. As shown in Figure 4, as the mini-batch size enlarges, the proportion impacted increases with 32-bit precision. However, with 64-bit precision, none of the sampled network parameters fell in the numerical bifurcation zone.

**Impact of network size:** We investigated the impact of varying depths of VGG networks (11, 13, 16, 19) on the percentage of affected mini-batches in  $S$ . Figure 4 shows that network depth does not significantly affect the proportion of impacted mini-batches in  $S$  at 16-bit and 32-bit precisions.

**Impact of batch-normalization:** Figure 4 shows a marked rise in affected mini-batches with batch normalization for 32-bit precisions.

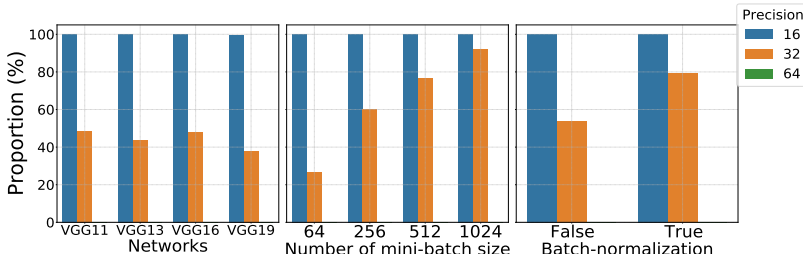


Figure 4: Impact of different size parameters on the proportion of affected mini-batches (Equation (19)) using CIFAR10 dataset. First: Different VGG network sizes. Second: VGG11 with varying mini-batch sizes. Third: VGG11 with and without batch normalization.

## 4 Impact on learning

### 4.1 Benchmarks and implementation

**Datasets and architectures:** We train neural networks to investigate the impact of numerical effects outlined in Section 3. Our experiments used CIFAR10 [33], MNIST [36] and ImageNet [16] datasets. We test various network architectures including VGG11 [44], ResNet [25], and LeNet [36]. Comprehensive details are available in Appendix C.1.

**Training settings:** The default optimizer is SGD. We investigate the effect of batch normalization, Adam optimizer [32], and different floating-point precisions (16-bit, 32-bit, mixed-precision [39]). The experiments were conducted using the PyTorch [41] framework, and we utilized Nvidia V100 GPUs for this purpose. Let  $(B_k)_{k \in \mathbb{N}}$  denote a sequence of mini-batches with sizes  $|B_k| \subset \{1, \dots, N\}$  for all  $k$  and  $\alpha_k > 0$  the learning rate. Let  $P = \{P_i\}_{i=1}^N$  be a program implementing a neural network. More precisely, for each  $i = 1, \dots, N$ ,  $P_i$  implement a composition function  $l_i$  as in Definition 1. Given initial network parameters  $\theta_{0,P}$ , the SGD training procedure of  $P$  consists in applying the recursion

$$\theta_{k+1,P} = \theta_{k,P} - \gamma \frac{\alpha_k}{|B_k|} \sum_{i \in B_k} \text{backprop}[P_i](\theta_{k,P}) \quad (16)$$

where  $\gamma > 0$  is a step-size parameter. Note that we explicitly wrote the sequence dependency in a program  $P$ .

### 4.2 Effect on training and test errors

We first consider training a VGG11 architecture on CIFAR10 using the SGD optimizer. For hybrid MaxPool-derived programs (see Definition 6), we train the network ten times with random initializations under 16 and 32-bit precision for different values of  $\beta$ . The results are reported in Figure 5. It is worth noting that a revised version of [4] exists. Our findings are consistent with the results presented in this updated publication, whereas they did not align with the initial version.

**Training effect with 16-bit:** For  $\beta$  values greater than  $10^3$ , we observe training instability and exploding gradients, regardless of batch normalization. Stable and efficient test accuracy persists for  $\beta \in \{0, 1, 10, 100\}$ .

**Training effect with 32-bit:** When the value of  $\beta$  is large (e.g.  $10^4$ ), training can become unstable, leading to oscillations and sudden jumps in the learning process if batch normalization is not applied. However, using batch normalization with a large  $\beta$  value can prevent this issue, resulting in improved accuracy on test data and avoiding the problem of gradient explosion. Our findings remain consistent across different network architectures and datasets. However, the sensitivity to  $\beta$  varies (see Appendix C). Large  $\beta$  values can introduce chaos in training and negatively affect test accuracy. A default  $\beta = 0$  is effective, but not universal. Figure 5 illustrates the effect of  $\beta \in \{1, 10, 100\}$ . As cited in [4] for ReLU-derived programs, we also observed that using the Adam optimizer with 32-bit floating-point arithmetic helps mitigate the impact of large  $\beta$  on test errors and stabilizes fluctuations in training loss. Refer to Appendix C.2 for more details.

**Connection between training and network parameters differences:** We trained seven VGG11 networks,  $\{P_i\}_{i=0}^6$ , with 32-bit precision on CIFAR10, each for 200 epochs using 128-sized mini-batches, a constant learning rate  $\alpha_k = 1$ , and momentum  $\gamma \in [0.01, 0.012]$ . These networks, initialized with identical parameters, implemented varying hybrid MaxPool-derived programs  $\{\beta_i\}_{i=0}^6$ . We enabled nondeterministic GPU computation and measured backpropagation variations (see Definition 7) between the baseline  $P_0$  and others per epoch. Test accuracies were tracked, with results detailed in Figure 6. In nondeterministic GPU settings, parameter variations within two runs of VGG networks at  $\beta = 0$  are comparable to those between networks with  $\beta = 0$  and  $\beta \in \{1, 10, 10^2, 10^3\}$ .

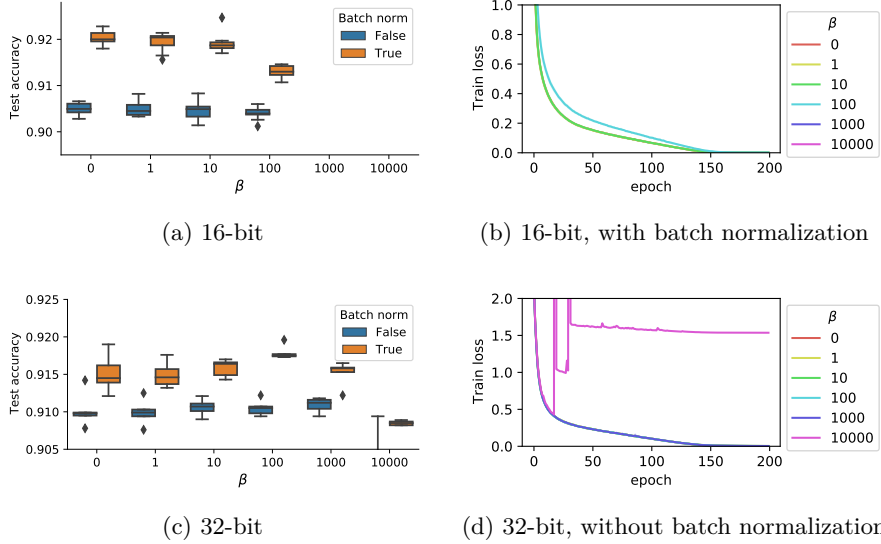


Figure 5: Training a VGG network on CIFAR10 with SGD. We performed ten random initializations for each experiment, depicted by the boxplots and the filled contours (standard deviation).

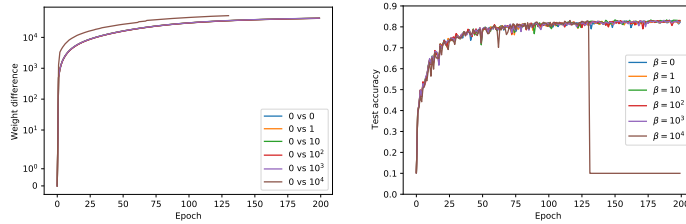


Figure 6: Left: Difference between network parameters ( $L^1$  norm) at each epoch. “0 vs 0” indicates  $\|\theta_{k,P_0} - \theta_{k,P_7}\|_1$  where  $P_7$  is a second run of  $P_0$  for sanity check, “0 vs 1” indicates  $\|\theta_{k,P_0} - \theta_{k,P_1}\|_1$ . Right: test accuracy of each  $\{P_i\}_{i=0}^5$  during 200 epochs.

Test accuracy remains stable for  $\beta$  values in this range, indicating insensitivity to  $\beta$  changes. However, at  $\beta = 10^4$ , we observe significant parameter divergence, linked to exploding gradients around epoch 130, leading to reduced test accuracy. This highlights that low  $\beta$  values maintain consistent convergence and don’t amplify nondeterministic GPU computation inconsistencies. Conversely, high  $\beta$  values risk destabilizing training.

## 5 Conclusion

This paper investigates the numerical reliability of automatic differentiation (AD) in neural networks containing MaxPool operations. The experiment investigates the effect of different precision levels of floating-point arithmetic on AD outputs. Several neural network models, such as LeNet, VGG, and ResNet, are tested across several datasets, including MNIST, CIFAR10, and ImageNet. Our research indicates that AD can produce inaccurate results when used with MaxPool operations on floating-point arithmetic in neural networks. This suggests that [37] findings may not apply to convolutional neural networks using MaxPool.

We focus on two key subsets of network parameters: the bifurcation zone and the compensation zone. The bifurcation zone is where both real and floating-point calculations in automatic differentiation (AD) is incorrect. In contrast, the compensation zone involves correct real number calculations but potential errors with floating-point numbers. Numerically, the bifurcation zone is rare with

notable amplitude fluctuations in backpropagation, while the compensation zone, more frequent, exhibits minor amplitude changes around machine precision due to rounding.

The selection of nonsmooth MaxPool Jacobians impacts the numerical stability of AD. Jacobians with lower norms lead to steadier training and improved test accuracy, while those with higher norms cause instability. This effect is especially significant in low-precision environments like 16-bit precision. Factors like dataset choice, network architecture, and learning settings, including batch normalization and the Adam optimizer, play a role in influencing AD’s numerical behavior and controlling gradient explosion.

## Acknowledgments and Disclosure of Funding

The author acknowledges the support of the AI Interdisciplinary Institute ANITI funding under the grant agreement ANR-19-PI3A-0004. The author acknowledges the help of the Association Nationale de la Recherche et de la Technologie (ANRT) and Thales LAS France, which contributed to Ryan B’s grant. This work was performed using HPC resources from CALMIP (Grant 2023-[P23040]). I thank Jérôme Bolte and Edouard Pauwels for helpful advice and suggestions. I thank my collaborators in the Thales LAS France, especially Beatrice Pesquet-Popescu and Andrei Purica, for their helpful comments.

## References

- [1] Martin Abadi, Paul Barham, Jianmin Chen, Zhifeng Chen, Andy Davis, Jeffrey Dean, Matthieu Devin, Sanjay Ghemawat, Geoffrey Irving, Michael Isard, Manjunath Kudlur, Josh Levenberg, Rajat Monga, Sherry Moore, Derek G. Murray, Benoit Steiner, Paul Tucker, Vijay Vasudevan, Pete Warden, Martin Wicke, Yuan Yu, and Xiaoqiang Zheng. Tensorflow: A system for large-scale machine learning. In *12th USENIX Symposium on Operating Systems Design and Implementation (OSDI 16)*, pages 265–283, 2016.
- [2] Paul I. Barton, Kamil A. Khan, Peter Stechliniski, and Harry A.J. Watson. Computationally relevant generalized derivatives: theory, evaluation and applications. *Optimization Methods and Software*, 33(4-6):1030–1072, 2018.
- [3] Atilim Gunes Baydin, Barak A Pearlmutter, Alexey Andreyevich Radul, and Jeffrey Mark Siskind. Automatic differentiation in machine learning: a survey. *Journal of Machine Learning Research*, 18:1–43, 2018.
- [4] David Bertoin, Jérôme Bolte, Sébastien Gerchinovitz, and Edouard Pauwels. Numerical influence of  $\text{relu}'(0)$  on backpropagation, 2023.
- [5] Jérôme Bolte, Ryan Boustany, Edouard Pauwels, and Béatrice Pesquet-Popescu. On the complexity of nonsmooth automatic differentiation. In *The Eleventh International Conference on Learning Representations*, 2022.
- [6] Jérôme Bolte, Tam Le, Edouard Pauwels, and Antonio Silveti-Falls. Nonsmooth implicit differentiation for machine learning and optimization. *CoRR*, abs/2106.04350, 2021.
- [7] Jérôme Bolte, Tam Le, Edouard Pauwels, and Tony Silveti-Falls. Nonsmooth implicit differentiation for machine-learning and optimization. *Advances in Neural Information Processing Systems*, 34, 2021.
- [8] Jérôme Bolte and Edouard Pauwels. Conservative set valued fields, automatic differentiation, stochastic gradient methods and deep learning. *Mathematical Programming*, pages 1–33, 2020.
- [9] Jérôme Bolte and Edouard Pauwels. A mathematical model for automatic differentiation in machine learning. In *Conference on Neural Information Processing Systems*, 2020.

- [10] Léon Bottou, Frank E Curtis, and Jorge Nocedal. Optimization methods for large-scale machine learning. *Siam Review*, 60(2):223–311, 2018.
- [11] James Bradbury, Roy Frostig, Peter Hawkins, Matthew James Johnson, Chris Leary, Dougal Maclaurin, George Necula, Adam Paszke, Jake VanderPlas, Skye Wanderman-Milne, and Qiao Zhang. JAX: composable transformations of Python+NumPy programs, 2018.
- [12] Frank H Clarke. *Optimization and nonsmooth analysis*. SIAM, 1983.
- [13] Matthieu Courbariaux, Yoshua Bengio, and Jean-Pierre David. Training deep neural networks with low precision multiplications. In *Proceedings of the International Conference on Learning Representations*, 2015.
- [14] D. Davis, D. Drusvyatskiy, S. Kakade, and J. D. Lee. Stochastic subgradient method converges on tame functions. *Foundations of Computational Mathematics.*, 2018.
- [15] Damek Davis, Dmitriy Drusvyatskiy, Sham Kakade, and Jason D Lee. Stochastic subgradient method converges on tame functions. *Foundations of computational mathematics*, 20(1):119–154, 2020.
- [16] Jia Deng, Wei Dong, Richard Socher, Li-Jia Li, Kai Li, and Li Fei-Fei. Imagenet: A large-scale hierarchical image database. In *2009 IEEE conference on computer vision and pattern recognition*, pages 248–255, 2009.
- [17] Ian Goodfellow, Yoshua Bengio, and Aaron Courville. *Deep learning*. MIT press, 2016.
- [18] A. Griewank and A. Rojas. Treating artificial neural net training as a nonsmooth global optimization problem. In *International Conference on Machine Learning, Optimization, and Data Science (pp. 759-770)*. Springer, Cham., 2019.
- [19] A. Griewank and A. Walther. Beyond the oracle: Opportunities of piecewise differentiation. In *Numerical Nonsmooth Optimization (pp. 331-361)*. Springer, Cham., 2020.
- [20] Andreas Griewank. On stable piecewise linearization and generalized algorithmic differentiation. *Optimization Methods and Software*, 28, 07 2013.
- [21] Andreas Griewank and Andrea Walther. *Evaluating derivatives: principles and techniques of algorithmic differentiation*. SIAM, 2008.
- [22] Andreas Griewank, Andrea Walther, Sabrina Fiege, and Torsten Bosse. On lipschitz optimization based on gray-box piecewise linearization. *Mathematical Programming*, 158:383–415, 2016.
- [23] Suyog Gupta, Ankur Agrawal, Kailash Gopalakrishnan, and Pritish Narayanan. Deep learning with limited numerical precision. In *International conference on machine learning*, pages 1737–1746. PMLR, 2015.
- [24] Kaiming He, Xiangyu Zhang, Shaoqing Ren, and Jian Sun. Delving deep into rectifiers: Surpassing human-level performance on imagenet classification. In *Proceedings of the IEEE international conference on computer vision*, pages 1026–1034, 2015.
- [25] Kaiming He, Xiangyu Zhang, Shaoqing Ren, and Jian Sun. Deep residual learning for image recognition. In *Proceedings of the IEEE conference on computer vision and pattern recognition*, pages 770–778, 2016.
- [26] Sepp Hochreiter and Jürgen Schmidhuber. Long short-term memory. *Neural Computation*, 9:1735–1780, 1997.
- [27] Gao Huang, Zhuang Liu, Laurens van der Maaten, and Kilian Q Weinberger. Densely connected convolutional networks. *Proceedings of the IEEE conference on computer vision and pattern recognition*, pages 4700–4708, 2017.

- [28] Kyuyeon Hwang and Wonyong Sung. Fixed-point quantization of deep convolutional networks. In *Proceedings of the International Conference on Machine Learning*, 2014.
- [29] Sergey Ioffe and Christian Szegedy. Batch normalization: Accelerating deep network training by reducing internal covariate shift. *arXiv preprint arXiv:1502.03167*, 2015.
- [30] Xianyan Jia, Shutao Song, Wei He, Yangzihao Wang, Haidong Rong, Feihu Zhou, Liqiang Xie, Zhenyu Guo, Yuanzhou Yang, Liwei Yu, et al. Highly scalable deep learning training system with mixed-precision: Training imagenet in four minutes. *arXiv preprint arXiv:1807.11205*, 2018.
- [31] Sham M Kakade and Jason D Lee. Provably correct automatic sub-differentiation for qualified programs. In *Advances in Neural Information Processing Systems*, volume 31. Curran Associates, Inc., 2018.
- [32] Diederik P Kingma and Jimmy Ba. Adam: A method for stochastic optimization. *arXiv preprint arXiv:1412.6980*, 2014.
- [33] Alex Krizhevsky and Geoff Hinton. Convolutional deep belief networks on cifar-10. *Unpublished manuscript*, 40(7):1–9, 2010.
- [34] Alex Krizhevsky, Ilya Sutskever, and Geoffrey E Hinton. Imagenet classification with deep convolutional neural networks. In *Advances in neural information processing systems*, pages 1097–1105, 2012.
- [35] Yann LeCun, Yoshua Bengio, and Geoffrey Hinton. Deep learning. *nature*, 521(7553):436–444, 2015.
- [36] Yann LeCun, Léon Bottou, Yoshua Bengio, and Patrick Haffner. Gradient-based learning applied to document recognition. *Proceedings of the IEEE*, 86(11):2278–2324, 1998.
- [37] Wonyeol Lee, Sejun Park, and Alex Aiken. On the correctness of automatic differentiation for neural networks with machine-representable parameters, 2023.
- [38] Wonyeol Lee, Hangeol Yu, Xavier Rival, and Hongseok Yang. On correctness of automatic differentiation for non-differentiable functions. In *NeurIPS 2020-34th Conference on Neural Information Processing Systems*, 2020.
- [39] Paulius Micikevicius, Sharan Narang, Jonah Alben, Gregory Diamos, Erich Elsen, David Garcia, Boris Ginsburg, Michael Houston, Oleksii Kuchaiev, Ganesh Venkatesh, et al. Mixed precision training. *arXiv preprint arXiv:1710.03740*, 2017.
- [40] Yuval Netzer, Tao Wang, Adam Coates, Alessandro Bissacco, Bo Wu, and Andrew Y Ng. Reading digits in natural images with unsupervised feature learning. In *NIPS workshop on deep learning and unsupervised feature learning*, volume 2011, page 5, 2011.
- [41] Adam Paszke, Sam Gross, Francisco Massa, Adam Lerer, James Bradbury, Gregory Chanan, Trevor Killeen, Zeming Lin, Natalia Gimelshein, Luca Antiga, Alban Desmaison, Andreas Kopf, Edward Yang, Zachary DeVito, Martin Raison, Alykhan Tejani, Sasank Chilamkurthy, Benoit Steiner, Lu Fang, Junjie Bai, and Soumith Chintala. Pytorch: An imperative style, high-performance deep learning library. In H. Wallach, H. Larochelle, A. Beygelzimer, F. d'Alché-Buc, E. Fox, and R. Garnett, editors, *Advances in Neural Information Processing Systems 32*, pages 8024–8035. Curran Associates, Inc., 2019.
- [42] D. E. Rumelhart, Geoffrey E. Hinton, and R. J. Williams. Learning representations by back-propagating errors. *Nature*, 323:533–536, 1986.
- [43] David E Rumelhart, Geoffrey E Hinton, and Ronald J Williams. Learning representations by back-propagating errors. *nature*, 323(6088):533–536, 1986.

- [44] Karen Simonyan and Andrew Zisserman. Very deep convolutional networks for large-scale image recognition. *arXiv preprint arXiv:1409.1556*, 2014.
- [45] Bert Speelpenning. *Compiling fast partial derivatives of functions given by algorithms*. University of Illinois at Urbana-Champaign, 1980.
- [46] Vincent Vanhoucke, Andrew Senior, and Mark Z Mao. Improving the speed of neural networks on cpus. In *Proceedings of the Deep Learning and Unsupervised Feature Learning Workshop*, 2011.
- [47] Kouichi Yamaguchi, Kenji Sakamoto, Toshio Akabane, and Yoshiji Fujimoto. A neural network for speaker-independent isolated word recognition. In *ICSLP*, 1990.
- [48] Matthew D Zeiler and Rob Fergus. Visualizing and understanding convolutional networks. In *European conference on computer vision*, pages 818–833, 2014.

This is the appendix for "On the numerical reliability of nonsmooth autodiff: a MaxPool case study".

## Contents

<b>A Further comments, discussion, and technical elements</b>	<b>16</b>
<b>B Proof related to Section 2.3</b>	<b>20</b>
<b>C Complements on experiments</b>	<b>20</b>
<b>D Complementary information</b>	<b>22</b>

## A Further comments, discussion, and technical elements

### A.1 Implementation of the zero program

The implementation of the zero function used in Table 1 is given in Figure 7. Programs  $\max_1$  and  $\max_2$  correspond to an equivalent implementation of the same function  $\max$ , but the computed derivatives are different.

```

def max1(x):
    # Derivative: first coordinate
    # Not the default in Torch
    res = x[0]
    for i in range(1, 4):
        if x[i] > res:
            res = x[i]
    return res

def max2(x):
    # Derivative: min norm
    # Default in Jax
    return torch.max(x)

def zero(t):
    # Zero function
    z = t * x
    return max1(z) - max2(z)

```

Figure 7: Implementation of programs  $\max_1$ ,  $\max_2$  and zero using Pytorch. Programs  $\max_1$  and  $\max_2$  are an equivalent implementation of  $\max$ , but with different derivatives due to the implementation.

### A.2 Challenges posed by MaxPool in image processing

In Convolutional Neural Networks (CNNs), the MaxPool operation is frequently used for reducing dimensions and downsampling. This function is especially crucial in image contexts, where uniform intensity regions are common, especially around the edges of objects and flat surfaces. One common situation is encountering identical pixel values within a pooling window, as shown in Figure 8. MaxPool must choose among these equivalent values, creating a point of non-differentiability. During training, this affects gradient calculation in backpropagation, affecting the updates to convolutional filters [17].

### A.3 AD errors with ReLU-derived programs

We conduct a small experiment in PyTorch [41] using the nonsmooth function  $\text{ReLU}: x \mapsto \max(x, 0)$ . Consider two programs  $\max_1$  and  $\max_2$  implementing the  $\max: x \mapsto \max_{1 \leq i \leq 4} x_i \in \mathbb{R}$  function using different ReLU-derived programs. Note that  $2 \max(x, y) = (x + y) + (\text{ReLU}(x) - \text{ReLU}(-y)) + (\text{ReLU}(y) - \text{ReLU}(-x))$ . Let  $\text{zero}_2: t \mapsto \max_1(t \times x) - \max_2(t \times x)$  be a program implementing the null function as described in Figure 9. Let  $\text{zero}'_2$  denote the backward AD algorithm for the zero program. As mathematical functions,  $\max_1$  and  $\max_2$  are equal and the program zero outputs

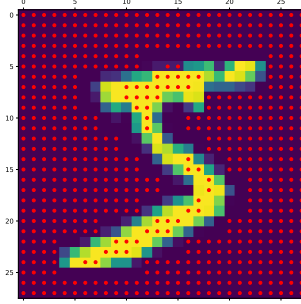


Figure 8: Image segment post-convolution, spotlighting equal pixel values (marked in red) within a 2x2 MaxPool window.

constantly 0. However, for some  $t \in \mathbb{R}$ , AD can return  $\text{zero}'_2(t) \neq 0$ . Results are reported in Table 3 and similar to Table 1.

```
def relu(x):
    return torch.relu(x)

def relu2(x):
    return torch.where(x >= 0, x, torch.tensor(0.0))

def max01(x):
    return (x[0] + x[1]) / 2 + relu((x[0] - x[1]) / 2) + relu((x[1] - x[0]) / 2)

def max02(x):
    return (x[0] + x[1]) / 2 + relu2((x[0] - x[1]) / 2) + relu((x[1] - x[0]) / 2)

def max1(x):
    return max01(torch.stack([max01(x[0:2]), max01(x[2:4])]))

def max2(x):
    return max02(torch.stack([max02(x[0:2]), max02(x[2:4])]))

def zero_2(t):
    z = t * x
    return max1(z) - max2(z)
```

Figure 9: Implementation of  $\text{max}_1$ ,  $\text{max}_2$  and  $\text{zero}_2$  using Pytorch. Programs  $\text{max}_1$  and  $\text{max}_2$  are an equivalent implementation of  $\text{max}$ , but implemented using different ReLU-derived programs.

$t$					$\text{zero}'_2(t)$						
					$-10^{-3}$	$-10^{-2}$	$-10^{-1}$	0	$10^1$	$10^2$	$10^3$
$x =$	1.0	2.0	3.0	4.0	0.0	0.0	0.0	1.5	0.0	0.0	0.0
$x =$	1.4	1.4	1.4	1.4	$10^{-7}$	$10^{-7}$	$10^{-7}$	$10^{-7}$	$10^{-7}$	$10^{-7}$	$10^{-7}$

Table 3: Summary of various types of AD errors with  $\text{zero}_2$  program using PyTorch for different combinations of  $t$  and  $x$ .

## A.4 NormPool : a nonsmooth multivariate operation without compensation errors

We conducted an experiment to show that compensation errors are not caused by the multivariate nature of nonsmooth elementary functions when using floating-point arithmetic. In this experiment, we used the NormPool operation, which is similar to the MaxPool operation but replaces the maximum with the Euclidian norm. Two programs,  $P$  and  $Q$ , were used to implement a LeNet-5 network on the MNIST dataset with two different NormPool-derived programs. We computed the backprop variation (see Definition 7) between  $P$  and  $Q$ , while controlling all sources of divergence in our implementation using deterministic computation. The results are presented in Figure 10. The experiment was conducted on a CPU with 16-bit floating-point precision.

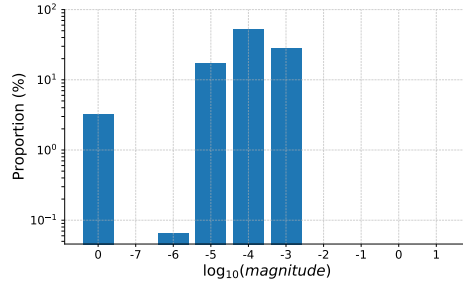


Figure 10: Histogram of backprop variation between  $P$  and  $Q$  for a LeNet-5 network on MNIST (128 mini-batch size) with 16-bit. We run  $M = 1000$  experiments.

In contrast to our findings with MaxPool, we obtained similar results to those reported in [4] with ReLU-based programs. Specifically, for NormPool-based programs, we observed either significant divergence of backprop or no variation.

## A.5 Bifurcation zone: a practical example

This section presents an example that demonstrates cases where AD can be incorrect. Calculating the accurate derivative for all inputs might be impossible, particularly when the function is nondifferentiable. This is because the derivative does not exist for inputs where the function is nondifferentiable.

### A.5.1 Network configuration

Consider an input matrix  $X$  of size  $4 \times 4$  given by:

$$X = \begin{pmatrix} 1 & 0 & 0 & 1 \\ 0 & 0 & 0 & 0 \\ 0 & 0 & 0 & 0 \\ 0 & 0 & 0 & 0 \end{pmatrix} \quad (\text{Input})$$

Let  $k$  be a positive number and  $W$  be a convolution kernel of size  $3 \times 3$  given by:

$$W = k \cdot \begin{pmatrix} 1 & 1 & 1 \\ 1 & 1 & 1 \\ 1 & 1 & 1 \end{pmatrix} \quad (\text{Convolution kernel})$$

Let's consider a composition function  $l$  such that:

$$l(W) = \text{MaxPool} \circ (X * W) = k \quad (17)$$

where the convolution operation  $X * W$  produces an output matrix  $Z$  of size  $2 \times 2$ , followed by the application of a MaxPool with a pooling window of size  $2 \times 2$ .

### A.5.2 Backprop computation: native vs minimal

Let  $P$  (resp.  $Q$ ) be a program implementing the composition function  $l$  in Equation (17) using the native (resp. minimal) MaxPool-derived program. Then, we have:

$$\text{backprop}[P](W) = \begin{pmatrix} 1 & 0 & 0 \\ 0 & 0 & 0 \\ 0 & 0 & 0 \end{pmatrix}, \quad \text{backprop}[Q](W) = \begin{pmatrix} 0.5 & 0 & 0.5 \\ 0 & 0 & 0 \\ 0 & 0 & 0 \end{pmatrix}$$

The convolutional kernel  $W$  falls within the bifurcation zone defined in Definition 3.

## A.6 Comments on Section 3

### A.6.1 Non-determinism in GPU computation

Graphics Processing Units (GPUs) are designed for parallel processing, which can result in unpredictable behaviors.

- **Floating-point operations:** The non-associative nature of floating-point arithmetic can lead to discrepancies. These differences might become significant as they accumulate across operations.
- **Reduction operations:** Functions like sum or maximum, especially in GPUs, can exhibit variability between runs. This variability can result in divergent accumulated rounding errors.

### A.6.2 Threshold values for various networks in Section 3.1

Table 4 presents threshold values for various neural networks on different datasets, computed under different floating-point precisions (16-bit, 32-bit, and 64-bit). For simplicity, thresholds are approximated as powers of 10.

Network $f$	Dataset	$\tau_{f,16}^1$	$\tau_{f,16}^2$	$\tau_{f,32}^1$	$\tau_{f,32}^2$	$\tau_{f,64}^1$	$\tau_{f,64}^2$
LeNet-5	MNIST	0	$10^{-5}$	$10^{-6}$	$10^{-5}$	$10^{-14}$	0
VGG-11	CIFAR-10	0	$10^{-1}$	$10^{-8}$	$10^{-7}$	$10^{-14}$	0
VGG-11	SVHN	0	$10^{-1}$	$10^{-8}$	$10^{-7}$	$10^{-15}$	0
VGG-13	CIFAR-10	0	$10^{-1}$	$10^{-9}$	$10^{-9}$	$10^{-14}$	0
VGG-16	CIFAR-10	0	$10^{-2}$	$10^{-10}$	$10^{-9}$	$10^{-15}$	0
VGG-19	CIFAR-10	0	$10^{-3}$	$10^{-11}$	$10^{-10}$	$10^{-15}$	0
ResNet-18	CIFAR-10	$10^{-2}$	1	$10^{-3}$	$10^{-4}$	$10^{-13}$	0
DenseNet-121	CIFAR-100	0	$10^{-2}$	$10^{-6}$	$10^{-1}$	$10^{-14}$	0

Table 4: Threshold values of various neural networks  $f$  across different datasets.

### A.6.3 Details on Monte Carlo sampling in Section 3.2

Recall that, for a neural network  $f$  and a floating-point precision  $\omega$ , we want to estimate the volume of the set

$$S(\tau_{f,\omega}) = \{\theta \in \mathbb{R}^P : \exists i \in \{1, \dots, N\}, \|\text{backprop}[P_i](\theta) - \text{backprop}[Q_i](\theta)\|_1 > \tau_{f,\omega}\} \subset \Theta_B$$

Our experiments divide a dataset into  $R$  mini-batches. Each  $r$ -th mini-batch is represented by the index set  $B_r \subset \{1, \dots, N\}$ . The programs  $P_r$  and  $Q_r$  are associated with the neural network  $f$  and implement a composition function  $l_r$  for each  $r$ . Specifically,  $P_r$  uses the native MaxPool-derived program, whereas  $Q_r$  uses the minimal one. For every precision level  $\omega \in \{16, 32, 64\}$ , we establish a

threshold  $\tau_{f,\omega}$  as in Section 3. Using the Kaiming-Uniform [24] initialization in PyTorch, we randomly generate a parameter set  $\{\theta_j\}_{j=1}^K$ , with  $K = 1000$ . The first line of Table 2 is given by the formula

$$\frac{1}{K} \sum_{k=1}^K \mathbb{1} \left( \exists r \in \{1, \dots, R\}, \left\| \text{backprop} \left[ \sum_{j \in B_r} P_j(\theta) \right] - \text{backprop} \left[ \sum_{j \in B_r} Q_j(\theta) \right] \right\|_1 > \tau_{f,\omega} \right), \quad (18)$$

where  $\mathbb{1}$  represents the indicator function, returning either 1 or 0 depending on the truth value of its argument’s condition. Similarly, the second line of Table 2 is given by the formula

$$\frac{1}{KR} \sum_{k=1}^K \sum_{r=1}^R \mathbb{1} \left( \left\| \text{backprop} \left[ \sum_{j \in B_r} P_j(\theta) \right] - \text{backprop} \left[ \sum_{j \in B_r} Q_j(\theta) \right] \right\|_1 > \tau_{f,\omega} \right), \quad (19)$$

Using the formula

$$\sqrt{\frac{\ln \left( \frac{2}{\alpha} \right)}{2n}},$$

and setting  $\alpha = 0.05$ , we compute the error margin of the Hoeffding confidence interval as  $n = K$  for Table 2’s first line and  $n = KR$  for its second. The first line adheres to a 95% confidence interval under the *iid* assumption due to Hoeffding’s inequality.

Using McDiarmid’s inequality at risk level  $\alpha = 0.05$ , we compute the error margin of the second line in Table 2 by the formula

$$\sqrt{\frac{1}{2} \left( \frac{1}{K} + \frac{1}{R} \right) \ln \left( \frac{2}{\alpha} \right)}.$$

## B Proof related to Section 2.3

### Proof of Proposition 1:

1. The three subsets have unique definitions, indicating that they are separate. For instance, a parameter cannot belong to the regular and bifurcation zones since the regular zone is defined as the area where each program  $g_{i,j}$  is assessed at differentiable points. On the other hand, the bifurcation zone is defined as the region where the set of all possible backprop outputs is not a singleton, indicating non-differentiability at some points. Additionally, the union of these zones covers the entire parameter space  $\Theta$  as every parameter must be assigned to one of the three subsets: resulting in differentiable points when evaluated, resulting in nondifferentiable points but having a singleton backprop set, or resulting in nondifferentiable points with a non-singleton backprop set. Therefore,  $\Theta_R \cup \Theta_B \cup \Theta_C = \Theta$ .
2. As we consider locally Lipschitz semialgebraic (or definable) functions, see [Theorem 1, [8]] for the proof arguments.

□

## C Complements on experiments

### C.1 Benchmark datasets and architectures

**Datasets:** In this work, we utilized various well-known image classification benchmarks. Below are the datasets, including their characteristics and original references.

Dataset	Dimensionality	Training set	Test set
MNIST	$28 \times 28$ (grayscale)	60K	10K
CIFAR10	$32 \times 32$ (RGB)	60K	10K
SVHN	$32 \times 32$ (RGB)	600K	26K
ImageNet	$224 \times 224$ (RGB)	1.3M	50K

The corresponding references for these datasets are [36, 33, 40].

**Neural network architectures:** We evaluated various CNN neural network architectures, with details as follows:

Name	Layers	Loss function
LeNet-5	5	Cross-entropy
VGG11	11	Cross-entropy
VGG13	13	Cross-entropy
VGG16	16	Cross-entropy
VGG19	19	Cross-entropy
ResNet18	18	Cross-entropy
ResNet50	50	Cross-entropy
DenseNet121	125	Cross-entropy

The corresponding references for these architectures are [44, 25, 27, 36].

**LeNet-5:** The implementation for LeNet-5 was sourced from the following GitHub repository: <https://github.com/ChawDoe/LeNet5-MNIST-PyTorch/blob/master/model.py>.

**VGG:** We used the PyTorch repository’s implementation for the VGG models. It can be accessed at the following link: <https://github.com/PyTorch/vision/blob/main/torchvision/models/vgg.py>.

**ResNet:** For ResNet models, we utilized the PyTorch repository’s implementation available at: <https://github.com/PyTorch/vision/blob/main/torchvision/models/resnet.py>. We made minor adjustments to the output layer’s size (changing from 1000 to 10 classes) and the kernel size in the primary convolutional, varying from 7 to 3). When batch normalization was not used, we replaced the batch normalization layers with identity mappings.

**DenseNet:** The implementation for DenseNet was taken from the PyTorch repository, available at: <https://github.com/PyTorch/vision/blob/main/torchvision/models/densenet.py>.

## C.2 Mitigating factor: Adam optimizer

After training a VGG11 network on CIFAR-10 using the Adam optimizer, we obtained results shown in Figure 11. Our findings are consistent with those presented in Section 3, but the network exhibits reduced sensitivity to  $\beta$ , resulting in improved stability of both test errors and training loss.

## C.3 Additional experiments with MNIST and LeNet-5 networks

We repeated the experiments in Section 4.2 using a LeNet-5 network on the MNIST dataset. The results are depicted in Figure 12. We found that for 16 bits, the test accuracies were similar when training was possible, but  $\beta = \{10^3, 10^4\}$  caused chaotic training behavior. For 32 bits, the test accuracies were mostly similar, except for  $\beta = 10^4$ . We noticed that the chaotic oscillations had completely disappeared.

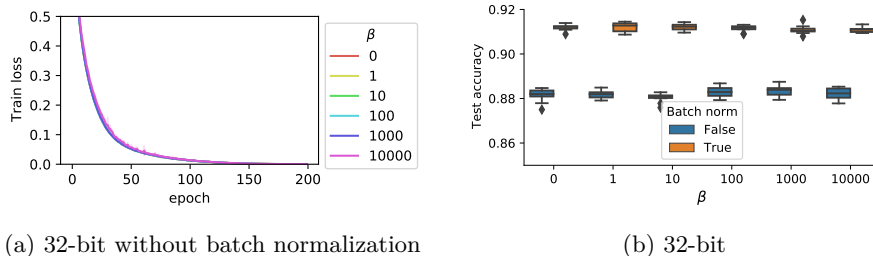


Figure 11: Training losses on CIFAR10 (left) and test accuracy (right) on VGG network trained with Adam optimizer and without batch normalization.

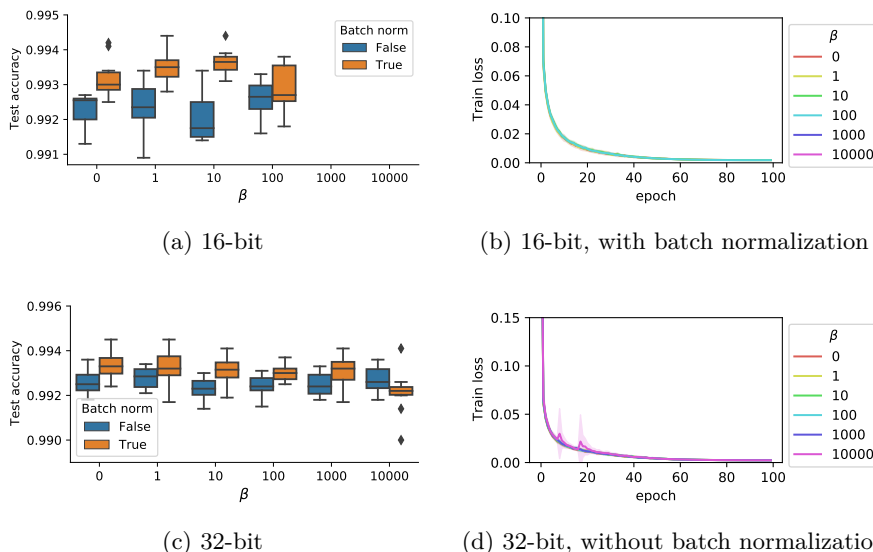


Figure 12: Training a LeNet-5 network on MNIST with SGD. We performed ten random initializations for each experiment, depicted by the boxplots and the filled contours (standard deviation).

#### C.4 Additional experiments with ResNet18

We performed the same experiments described in Section 4.2 using ResNet18 architecture trained on CIFAR 10. Figure 13 represents the test errors with or without batch normalization. For 16 bits, test accuracies are similar, but  $\beta = 10^4$  induces chaotic training behavior. For 32 bits, test accuracies are identical, and the chaotic oscillations phenomena have entirely disappeared.

#### C.5 Additional experiments with ResNet50 on ImageNet

We performed the same experiments described in Section 4.2 using a ResNet50 architecture trained on ImageNet. The test accuracy is represented in Figure 14. We employ mixed precision [39, 30], utilizing 16 and 32 bits precision to balance computational speed and information retention. Test accuracies are similar when training is possible, but  $\beta = 10^3$  induces chaotic training behavior.

### D Complementary information

**Computational Resources:** All the experiments were conducted on four Nvidia V100 GPUs. This ensured consistent and reliable computation times across different experimental runs.

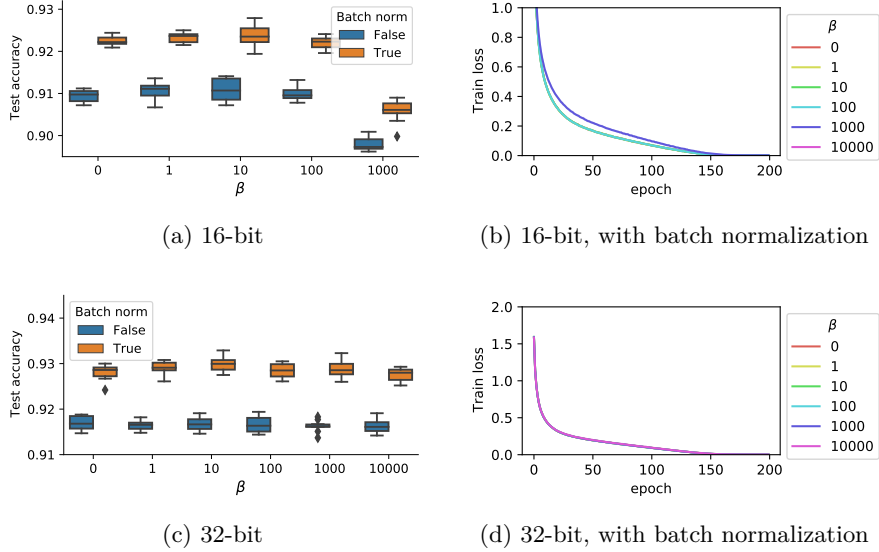


Figure 13: Training a ResNet18 network on CIFAR10 with SGD. We performed ten random initializations for each experiment, depicted by the boxplots and the filled contours (standard deviation).

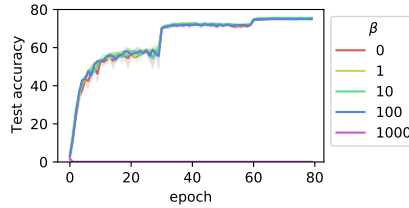


Figure 14: Test accuracy during training a Resnet50 on ImageNet with SGD using mixed precision. The shaded area represents three runs. We have a chaotic test accuracy behavior for  $\beta = 10^3$ .

**Code and Results Availability:** The code corresponding to the experiments, as well as the results of these experiments, are publicly available. The repository can be accessed at the following URL: <https://github.com/ryanboustany/MaxPool-numerical>.

**Licenses:** The datasets used in our experiments are released under various licenses. CIFAR10 is under the MIT license, MNIST and SVHN are under the GNU General Public License, and ImageNet is under the BSD license. The libraries we used, Numpy and PyTorch, are released under the BSD license, while Python is released under the Python Software Foundation License.

Dataset	Network	Optimizer	Batch Size	Epochs	Time Per Epoch	Repetitions
MNIST	LeNet-5	SGD	128	100	2 seconds	10
CIFAR10	VGG11	SGD	128	200	9 seconds	10
CIFAR10	ResNet18	SGD	128	200	13 seconds	10
SVHN	VGG11	SGD	128	100	70 seconds	10
ImageNet	Resnet50	SGD	512	90	15 minutes	3

Table 5: Detailed experimental setup, including the dataset, neural network architecture, optimizer used, batch size, number of epochs, average computation time per epoch, and repetitions for each experiment.